JOM, Vol. 76, No. 2, 2024
https://doi.org/10.1007/s11837-023-06244-0

New Generation Wrought Al-Ca-Mg Natural Composite Alloys as an Alternative to the 5000 Series Alloys

T.K. AKOPYAN ,[1,2,3] N.A. BELOV,[2] N.V. LETYAGIN,[2] A.S. FORTUNA,[2] and X.D. NGUEN[2]

1.—Moscow Polytechnic University, 38, Bolshaya Semyonovskaya str., Moscow, Russia 107023.
2.—National University of Science and Technology MISIS, 4 Leninsky pr., Moscow, Russia 119049.
3.—e-mail: nemiroffandtor@yandex.ru

The structure and mechanical properties of the new group of wrought Al-3%Ca-(2-4)%Mg based alloys with a natural composite structure consisting of the aluminum matrix stabilized by homogenously distributed fine eutectic crystals of the Al_4Ca phase have been studied using theoretical and experimental analyses. The high-quality sheet metal obtained upon hot rolling at 400–450°C confirms the high processability of new materials. Deformation processing leads to the formation of fine sub-grain structure with a characteristic sub-grain size of 1 μm. Very fine crystals of the Al_4Ca phase particles are found at sub-grain boundaries, confirming their high pinning ability. Tensile tests of the as-wrought alloys revealed that addition of Ca in the Al-Mg alloys leads to a substantial increase in the strength properties (the ultimate tensile strength is in the 300–340 MPa range and the yield strengh is in 230–250 MPa range). Detailed analysis of various mechanisms influencing the strengthening of the new alloys revealed that contribution of sub-grain boundaries is the greatest and greatly exceeds all others: its contribution to the total YS is $> 60\%$. Thus, addition of eutectic forming calcium in wrought Al-Mg alloys allows one to increase the strength properties through the stabilization of the sub-grain structure.

INTRODUCTION

Al-Mg-Mn-based alloys are widely used in various industries, such as aerospace, marine, transportation and storage tanks, owing to their relatively high strength, good weldability and corrosion resistance.[1–4] The alloys of this group (5xxx series) are non-heat treatable, and they are mostly strengthened by solid solution hardening combined with strain hardening. An increase in the Mg content leads to an increase in the yield strength and tensile strength, indeed every 1% increment of Mg content in Al-Mg alloys can increase the tensile strength by 33 MPa.[5,6] However, with an increase in Mg content, a noticeable drop in the ductility is also observed. The latter fact complicates the processing and forming of the alloys. In addition, Al-Mg alloys with a magnesium content of $> 4\%$, before processing, should be treated by prolonged homogenization annealing,[7,8] which leads to additional time and energy consumptions.

On the other hand, many studies have appeared recently considering calcium as a promising additive in new light alloys.[9–12] Ca forms an eutectic system with aluminum (the eutectic point at 7.6 wt.% Ca and 617°C) and has a low density both in the pure metal (1.55 g/sm^3) and in the intermetallic Al_4Ca compound (2.35 g/sm^3). Because the fraction of the Al_4Ca phase in the eutectic reaches 30 vol.% (at $\sim$ 7.6 wt.% Ca), the Al-Ca alloys can be considered natural composites. In addition, Ca bounds the main Fe and Si impurities in the Al_2CaSi_2 and $Al_{10}CaFe_2$ ternary compounds forming in the multi-phase eutectics and having a finer structure[13,14] than Fe- and Si-containing phases, e.g., Al_3Fe, Al_5FeSi, etc., which are common for most aluminum alloys. The latter fact allows one to use scrap and secondary raw materials for new alloy

(Received July 3, 2023; accepted October 17, 2023; published online November 13, 2023)

synthesis. Although the crystals of the Al_4Ca phase can be present in the structure in large amounts, their fine structure originating from the eutectic solidification gives the Al-Ca-based alloys a sufficient deformation capacity, allowing one to obtain rolled sheets and wires.[15–17] For instance, a new Ca-containing alloy with a high fraction of both 0.5% Fe and 0.25% Si obtained at a high cooling rate during solidification was subjected to cold forming (both drawing and rolling) without preliminary annealing.[15] In earlier studies,[16,17] Al-Ca based alloys containing ~ 3–4 wt.% Ca obtained at conventional cooling rates possessed high processability at hot rolling and drawing without preliminary annealing although the volume fraction of the Ca-containing extra phase was > 15%.

To date, some studies have also been performed for the Al-Ca-Mg-based alloys. In a study,[18] we showed the possibility of designing new aluminum alloys based on Al-Ca-Mg(-Si) systems with a high magnesium content. It was shown that Ca and Si addition in Al-10% Mg alloy increases the hardness, reduces the density and has no negative influence on the corrosion resistance. In another study,[19] calcium addition up to 1 wt.% in Al-Mg-Sc-based alloy yielded a noticeable increase in the alloy heat resistance. In Refs. 20 and 21, the authors studied a new group of casting alloys based on the Al-Mg-Ca-(Zn) systems. In an earlier study,[20] the authors analyzed the effects of calcium and zinc additions on the phase equilibria and structural peculiarities of the eutectic phases of the Al-Ca alloys with a high magnesium content of ~ 6 wt.% Mg. Based on the reported results, the authors argued that Zn has a high solubility in the Al_4Ca phase and affects the morphology of the compound. In another study,[21] the authors confirmed the possibility of hardening in Al-Mg-Ca-based alloys by the Sc microaddition.

Thus, although there have been some studies of the Al-Ca-Mg system and alloys, no systematic studies of the wrought Al-Ca-Mg alloys have been conducted. Therefore, in this work we deal with a new group of wrought Al-Ca-Mg alloys with a natural composite structure. The composite structure results from the combination of the magnesium-alloyed aluminum matrix and eutectic crystals of the Al_4Ca phase. The main distinctive feature of the new alloys is a low or moderate content of Mg (up to 3 wt.%) at about the same content of calcium. The new alloys can be considered as a replacement for the conventional highly alloyed 5xxx alloys (5056 type), however having some advantages against the latter ones. For instance, much lower content of magnesium ensures a high processability of the new alloys at deformation treatment, and the fine structure of the Ca-containing eutectic particles provides additional strengthening, which is shown in this work to originate from the stabilization of the subgrain structure formed at hot deformation.

MATERIALS AND METHODS

The main test materials of this study were four alloys whose chemical compositions, according to spectral analysis made using an electron microprobe analysis system (Oxford Instruments), are presented in Table I. The actual compositions are quite close to the target one. The melting was carried out in a GRAFICARBO resistance furnace in a graphite crucible from high-purity aluminum 1199 (99.99 wt.% Al). Aluminum was placed in the crucible, and after its melting, Al-15%Ca and Al-10%Mn binary master alloys and pure magnesium (99.9%) were added to the melt. After melting the main components, the melt was held for 5–10 min to obtain a homogeneous composition, and the metal was cast into 10 × 20 × 180 mm graphite molds at 780–800°C. The cooling rate in the molds was about 10 K/s.

The optimal deformation temperature for the new alloys was chosen empirically based on test results for different hot rolling modes aiming to produce high-quality sheets without surface defects or typical edge cracks. Thus, the obtained ingots without preliminary annealing were subjected to hot rolling at 400°C for the Al3Ca2Mg alloy and at 450°C for the Al3Ca4Mg and Al3Ca2Mg0.7Mn alloys with an 80% reduction. For comparative analysis of the structural stability of the as-deformed alloys, the obtained 2 mm sheet samples were subjected to annealing at 250°C for different holding times. One should note that the most heat-resistant precipitation-hardened aluminum alloys soften rapidly during heating at > 225–250°C,[22] and therefore this temperature limit can be considered critical for the primary assessment of the thermal stability of the alloys. The specimens were annealed in a muffle electric furnace with a temperature accuracy of ~ 3 K.

The microstructure was examined using transmission electron microscopy (TEM, Jeol JEM 1400 microscope) and scanning electron microscopy (SEM, TESCAN VEGA 3) with an energy-dispersive x-ray spectroscopy analysis system (EDS, OXFORD Aztec, Oxford Instruments, Oxfordshire, UK) and Aztec software. Polished samples were used for the studies. The metallographic samples were ground with SiC abrasive paper and polished with 1 μm diamond suspension. One percent hydrogen fluoride (HF) water solution was used for etching. Thin foils for TEM were prepared by two-jet electrolytic polishing on a STRUERS Tenupol-5 installation at 21 V voltage. A solution of nitric acid in methanol in a ratio of 1:4 (vol.) cooled to − 15°C was used as an electrolyte.

The Vickers hardness (Hv) of the obtained hot-rolled sheets was measured using a DUROLINE MH-6 setup (METKON Instruments) with a load of 1 kg and dwell time of 10 s. At least five measurements were performed for each sample. The specific

Table I. Chemical composition of experimental alloys

Alloy designation	Concentration, wt.% (target/actual)				
	Al	Ca	Mg	Mn	Fe
Al3Ca2Mg	Balance	3.0/3.2	2.0/2.1	–/–	–/0.02
Al3Ca4Mg	Balance	3.0/3.1	4.0/4.1	–/–	–/–
Al3Ca2Mg0.7Mn	Balance	3.0/3.1	2.0/2.1	0.7/0.65	–/0.02

electrical conductivity (EC) of the samples was determined using the eddy current method with a VE-26NP eddy structurescope.

Room-temperature tensile tests were conducted for the peak-aged hot-rolled 2 mm sheets on a universal testing machine, model Zwick Z250 (the velocity of loading was 10 mm/min). Flat rectangular test samples without grippers having a length of 110 mm and width of 10 mm were made from hot-rolled 2 mm sheets. The strain rate was 5 mm/min.

To facilitate the preliminary analysis of the quaternary system, a thermodynamic calculation in the Thermo-Calc program and the TTAL5 database was initially conducted (TTAL5 databases[23,24]).

RESULTS

Theoretical and Experimental Analysis of As-cast Structure

Studies carried out earlier revealed that a calcium content of 3 wt.% allowed one to obtain a good balance of the strength and toughness properties of the alloys.[11,17,25,26] On the other hand, the 5049 type Al-Mg industrial alloy containing ~ 2%Mg possesses high processability upon deformation but has moderate strength. The Al-3Ca-2 Mg (wt.%) composition was chosen as the basic one for designing a new alloy. Preliminary analysis of the phase composition was made for the new composition using thermodynamic calculations in the Thermo-Calc program. As was shown Ref. 18, no compounds can be expected to be formed simultaneously by Ca and Mg in the Al-Ca-Mg based alloys. Due to the latter fact, only compounds pertaining to the corresponding binary systems can be expected in the ternary system. Indeed, according to the vertical isopleth presented in Fig. 1a, the solidification of the chosen Al3Ca2Mg alloy in the Al-3Ca-(0-5)Mg system starts from the formation of the primary aluminum solid solution followed by the $L \rightarrow (Al) + Al_4Ca$ binary eutectic. The solidification ends in the binary $(Al) + Al_4Ca$ phase field where magnesium is completely dissolved in aluminum.

Analysis of non-equilibrium solidification using Shiel-Gulliver simulation (Fig. 1b) revealed the appearance of the Al_3Mg_2 phase as part of the ternary non-equilibrium $L \rightarrow (Al) + Al_4Ca + Al_3Mg_2$ eutectic. The formation of the latter phase leads to a significant drop in the solidus temperature to ~ 450°C, which is close to the temperature of the $L \rightarrow (Al) + Al_3Mg_2$ binary eutectic in the Al-Mg system. The thermal analysis data (Fig. 1c) for this alloy correspond well to the Shiel-Gulliver simulation. Indeed, the solidification onset is detected at 630°C followed by binary eutectic solidification. Non-equilibrium solidification ends via a ternary eutectic at ~ 430°C. Considering the fact that undercooling always takes place at solidification, the experimentally determined temperatures of phase transformations correspond well to the calculated data (Fig. 1b).

The as-cast experimental Mg-containing alloys have a typical hypoeutectic structure consisting of the aluminum solid solution (Al) and eutectic crystals of the Al_4Ca phase (Fig. 2). However, unlike the Al-3Ca-based alloys studied earlier,[17,25] the eutectic structure of the new Al3CaMg-containing alloys appears to be coarse. Indeed, as shown earlier,[25] the eutectic colonies have an extremely fine structure, and no individual crystals of the Al_4Ca compound can be resolved by SEM. On the other hand, discrete crystals of the eutectic phase can be easily seen in the new Mg-containing Al3Ca2Mg alloy at the magnification used (Fig. 2a). According to EDS data, about 1% Mg is dissolved in aluminum in the Al3Ca2Mg alloy (Table II). Further increase in the magnesium content to 4% affects the eutectic structure but only slightly (Fig. 2b). The EDS data suggest that about 2.65% Mg is dissolved in the aluminum solid solution of the ternary Al3Ca4Mg alloy.

As it is known Ref. 27, Mn addition in Al-Mg alloys allows one to increase the strength because of solid solution hardening or via the formation of relatively fine Al_6Mn dispersoids (the characteristic size is several hundreds of nanometers). The dispersoids formed upon annealing or hot deformation of the specimens at 400–450°C cause pinning of the dislocations and sub-grain boundaries, thus preventing recrystallization.[28–30] In addition, in the presence of manganese, the formation of the $Al_6(Fe,Mn)$ phase with Chinese-script morphology instead of the needle-like Al_3Fe compound can be expected at solidification.[31] One should note that at an iron content typical of impurities and in the presence of excess calcium, the formation of compact $Al_{10}CaFe_2$ phase crystals instead of the Al_3Fe phase can be expected.[12,14] Normally, up to 1% Mn is

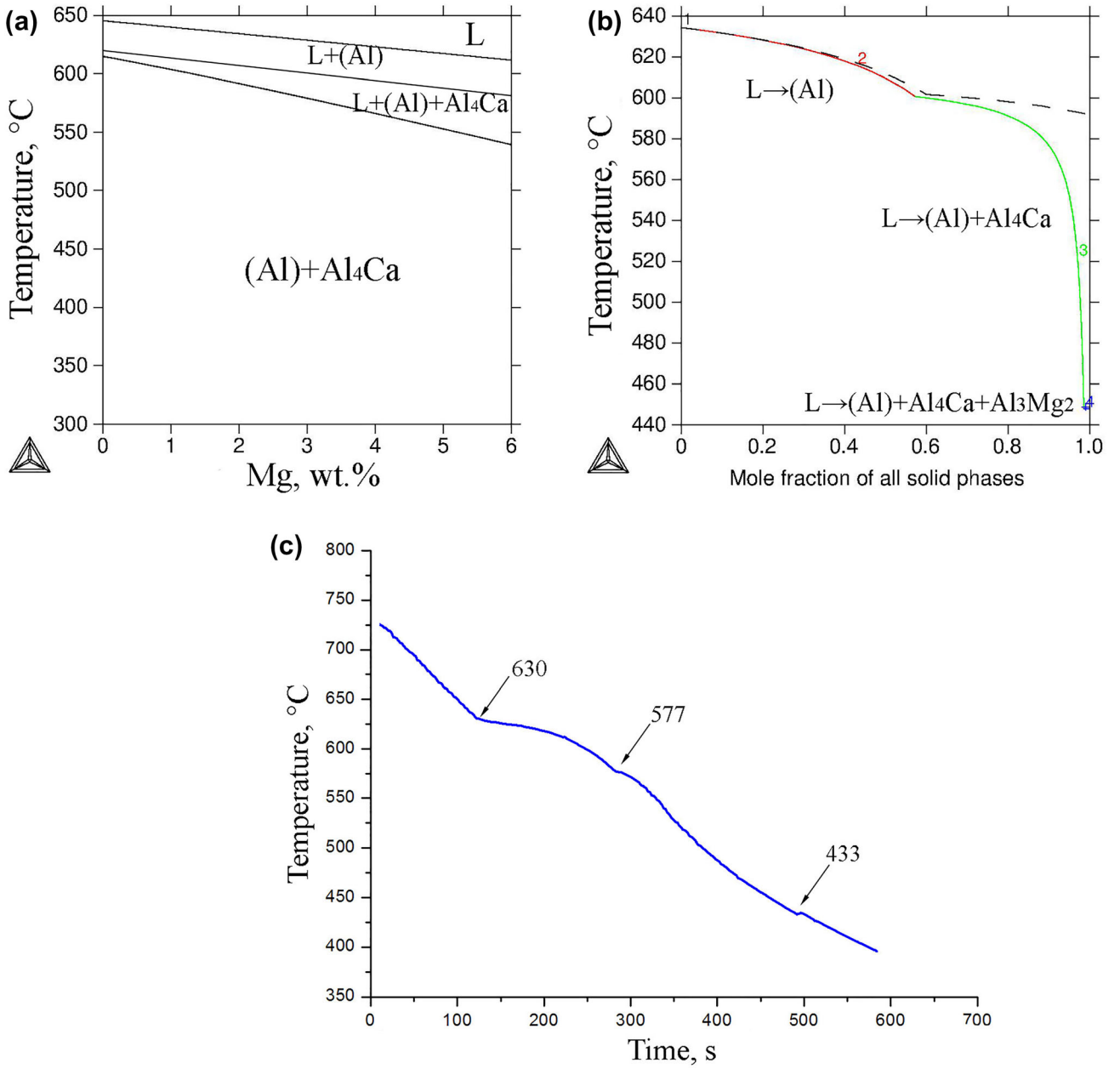

Fig. 1. (a) Vertical isopleth of the Al-3Ca-Mg system, (b) thermodynamic simulation of non-equilibrium solidification carried out using Shiel-Gulliver simulation for the Al3Ca2Mg alloy and (c) experimentally obtained cooling curve for the Al3Ca2Mg alloy.

added to the Al-Mg alloys.[1,4] In the current study, the influence of manganese at a content of 0.7% was considered for the model Al3Ca2Mg alloy. The as-cast structure of the new alloy is presented in Fig. 3. The morphology of the eutectic looks similar to that of the ternary Al3Ca2Mg alloy, but its distinctive feature is the presence (along with Al_4Ca phase crystals) of a minor fraction of fine bright crystals that are part of the eutectic (marked by arrows in Fig. 3b).

Elemental mapping illustrates (Fig. 3c) that all calcium is in the eutectic. The above-mentioned bright fine crystals in the eutectic are saturated with iron, which allows one to identify them as the Al_6(Fe,Mn) phase. Approximately, 0.7% Mn and 1.1% Mg are dissolved in the aluminum solid solution (Table II).

Influence of Hot Rolling on the Microstructure

The experimental alloys were subjected to hot rolling without preliminary homogenization annealing. The alloys were hot rolled at different temperatures depending on the chemical composition. Indeed, due to the relatively fine structure of the eutectic and low alloyed aluminum solid solution, the ternary Al3Ca2Mg alloy can be rolled at

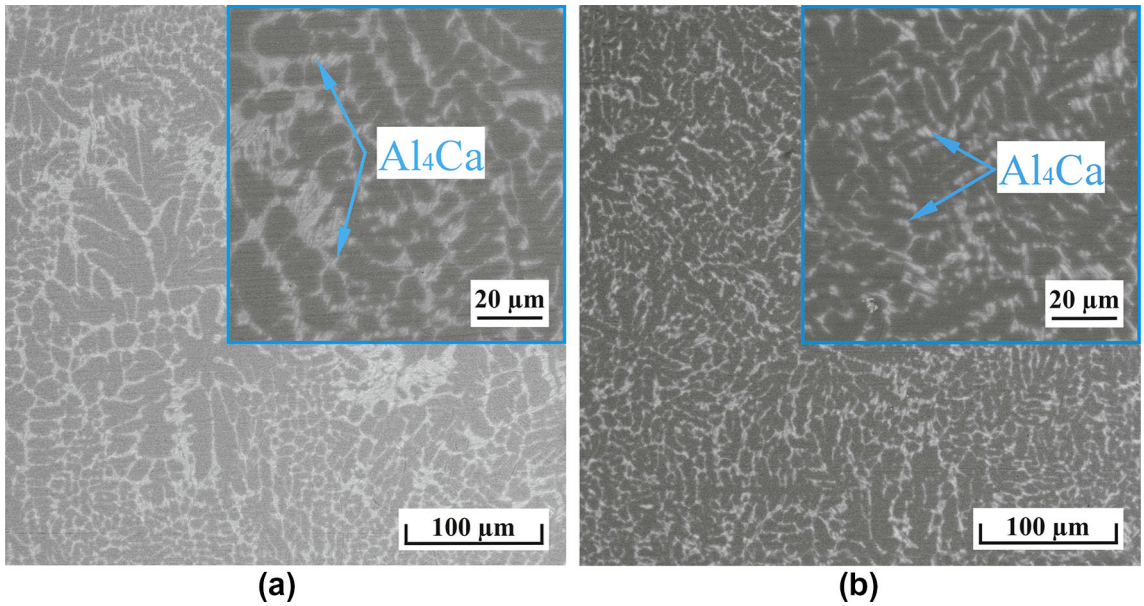

Fig. 2. SEM mictostructure of the experemental alloys in as-cast state: (a) Al3Ca2Mg and (b) Al3Ca4Mg. BSE.

Table II. Chemical composition of aluminum solid solution (EDS analysis)

	Chemical composition, wt.%		
Alloy	**Mg**	**Mn**	**Ca**
Al3Ca2Mg	0.99 ± 0.07	–	–
Al3Ca4Mg	2.65 ± 0.08	–	–
Al3Ca2Mg0.7Mn	1.10 ± 0.07	0.70 ± 0.1	–

relatively low temperatures of 350–400°C. Notably, according to the Thermo-Calc calculation, the fraction of the Al_4Ca eutectic phase is about 10%, which makes it possible to classify this alloy as a natural composite. The rather high workability of the deformed alloys at relatively high contents of the extra phase (for wrought aluminum alloys) is attributable to the relatively compact morphology and fine structure of these crystals. Manganese addition or an increase in the magnesium content leads to a substantial drop in the processability; thus, the remaining two experimental Al3Ca4Mg and Al3Ca2Mg0.7Mn alloys were rolled at a higher temperature, 450°C. Typical microstructures of these alloys after rolling are shown for the examples of the Al3Ca2Mg and Al3Ca2Mg0.7Mn alloys in Fig. 4. One can observe the formation of the fiber structure oriented in the rolling direction. The eutectic colonies are no longer observed, and the intermetallic particles of the Al_4Ca phase are uniformly distributed over the entire cross-section. Rolling also refines the eutectic crystals, whose the characteristic size is about 1–1.5 μm.

TEM analysis was used for a more detailed study of the deformed structure for the example of Al3Ca2Mg alloy. One can observe a severely deformed structure with different types of dislocation structure. The areas with extremely high density of tangled dislocations formed a so-called cell structure[4] having walls which contain these dislocations (Fig. 5a and b). This type of structure is more typical for cold working. However, along dislocation cells, the formation of fine sub-grains (Fig. 5c and d) with a characteristic size varying in the 0.5–1 μm range was observed. Very fine crystals (< 100 nm in size) are also found (marked by arrows) at cells and sub-grain boundaries, confirming their high pinning ability.

Tensile Tests and Hardness Analysis

The obtained hot-rolled sheets were subjected to hardness and electrical conductivity measurements and tensile tests. The hardness of the wrought alloys was also studied upon annealing at 250°C to reveal the thermal stability. As Fig. 6a shows, the base ternary Al3Ca2Mg alloy has a relatively high hardness of ~ 83 Hv in as-wrought state. However, an increase in the magnesium content to 4% substantially increases the hardness by ~ 25% to 100 Hv. Manganese addition also leads to an increase in the hardness but to a more moderate extent. Further annealing revealed more differences between the alloys. Indeed, at the beginning of annealing, the hardness of both ternary Al3Ca2Mg and Al3Ca4Mg alloys drops noticeably at about the same rates (the slope of this part of curves is nearly the same). After about 2 h annealing, the hardness drop rate for both alloys decreases; however, for the Al3Ca2Mg alloy it remains higher. For the Al3Ca4Mg alloy after ~ 8 h annealing, the hardness drops to ~ 80 Hv and then remains virtually

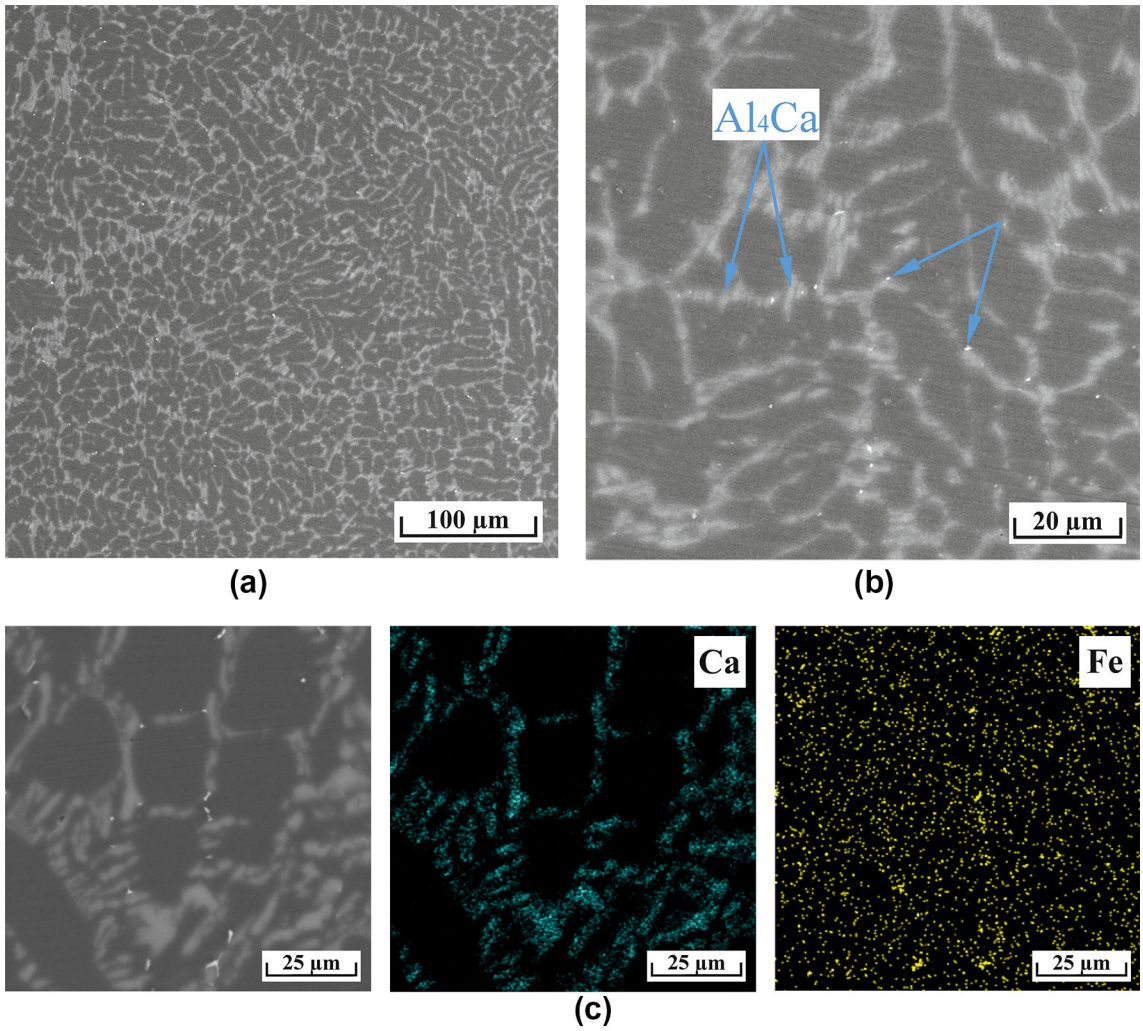

Fig. 3. As-cast structures of (a, b) the Al3Ca2Mg0.7Mn alloy and (c) elemental mapping obtained from the selected area (leftmost figure). SEM.

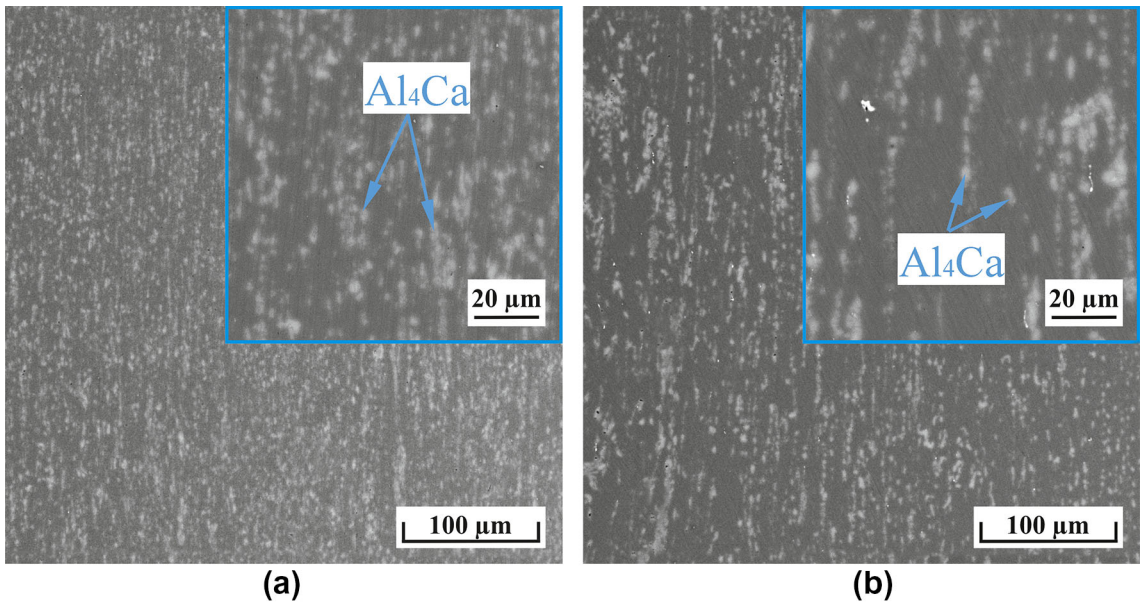

Fig. 4. SEM hot-rolled structure of (a) Al3Ca2Mg and (b) Al3Ca2Mg0.7Mn alloys. BSE.

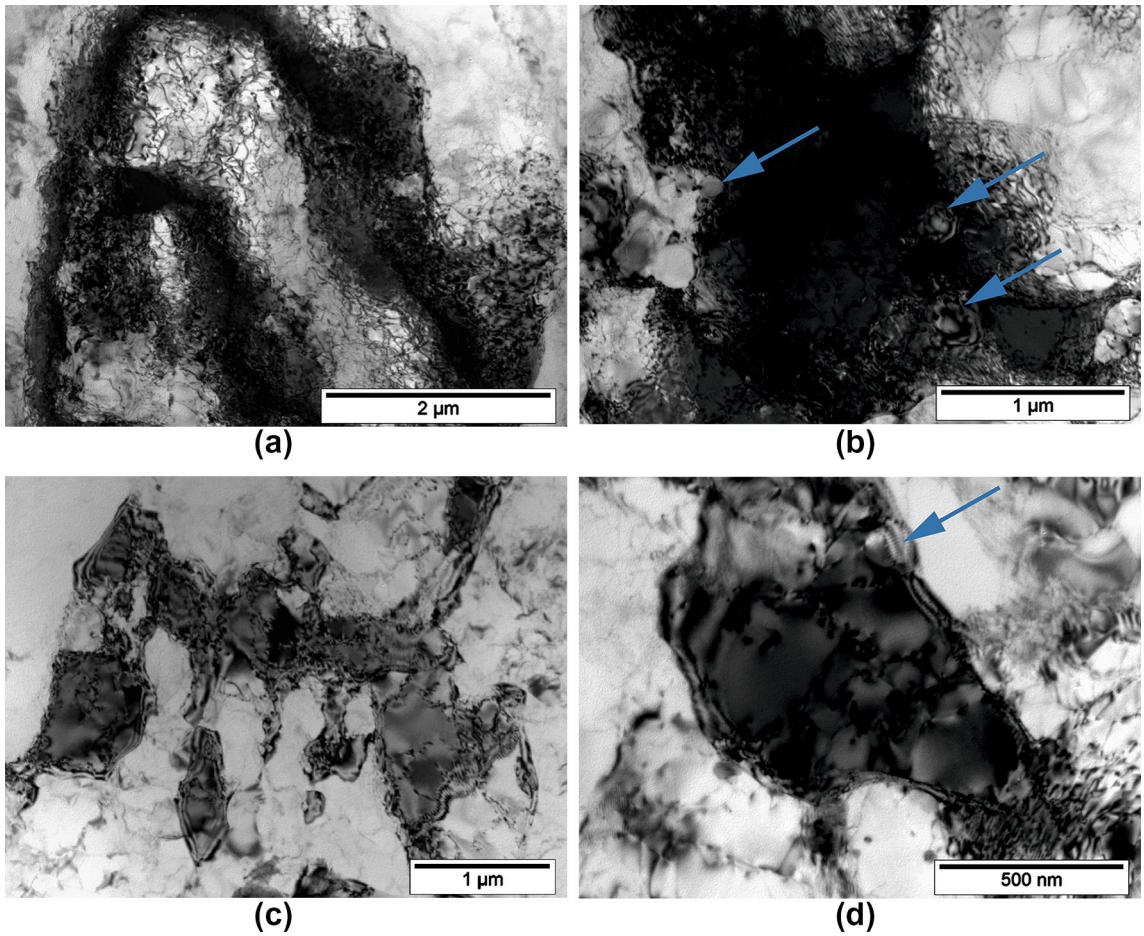

Fig. 5. TEM microstructure of the hot-rolled Al3Ca2Mg alloy. (a, b) High-density of tangled dislocations; (c, d) sub-grain structure.

unchanged for the rest of the time. The hardness of the Al3Ca2Mg alloy decreases gradually during the first 13 h of annealing to ~ 60 Hv and then also reaches a steady state. Thus, one can conclude from the experimental data on the hardness drop for the Al3Ca2Mg and Al3Ca4Mg alloys (27% vs. 20%) that magnesium addition can increase the thermal stability of the structure at annealing. However, manganese micro-addition is much more effective for this purpose. As seen for the Al3Ca2Mg0.7Mn alloy, the hardness drops slightly in the beginning by 5% and then remains almost unchanged, noticeably surpassing the hardness of the highly alloyed Al3Ca4Mg alloy.

Analysis of the specific electrical conductivity (EC) allows one to reveal phase transitions taking place during annealing (Fig. 6b). According to the obtained data, the EC of the studied alloys changes only slightly in time. The latter fact suggests that no phase transformation can take place at the 250°C annealing temperature used. Indeed, for both the Al3Ca2Mg and Al3Ca4Mg alloys, magnesium must be completely dissolved in the aluminum matrix. An increase in the magnesium content leads to a substantial decrease in the EC. However, the drop in the EC is even more significant for manganese addition. Indeed, the EC of the Al3Ca2Mg0.7Mn alloy is the lowest. The obtained result corresponds well with previous data[32] on the strong detrimental influence of manganese on the EC. Phase transformations associated with Mn (in particular, the formation of Al_6Mn dispersoids) can take place only at high temperatures (usually above 350°C), and the relatively lower 250°C annealing temperature is unable to influence them because of kinetic limitations.

The experimental alloys in the as-rolled state were also subjected to tensile tests without preliminary heat treatment. The obtained data were compared with the literature data[33] on the influence of hot rolling on the mechanical properties of the base Al-4%Mg alloy and ternary Al-4%Mg-Zr alloy containing 0.2%Zr. Typical initially obtained engineering stress-strain curves for the alloys are presented in Fig. 7a. The extracted data on the UTS, YS and relative elongation are presented as histograms in Fig. 7b, c, and d compared with literary data for the Al-4%Mg alloys. The serrated flow character of the obtained strain-stress curves was observed (Fig. 7a). The latter fact is evidence of the dynamic strain aging occurring during the deformation. Such an unstable plastic deformation

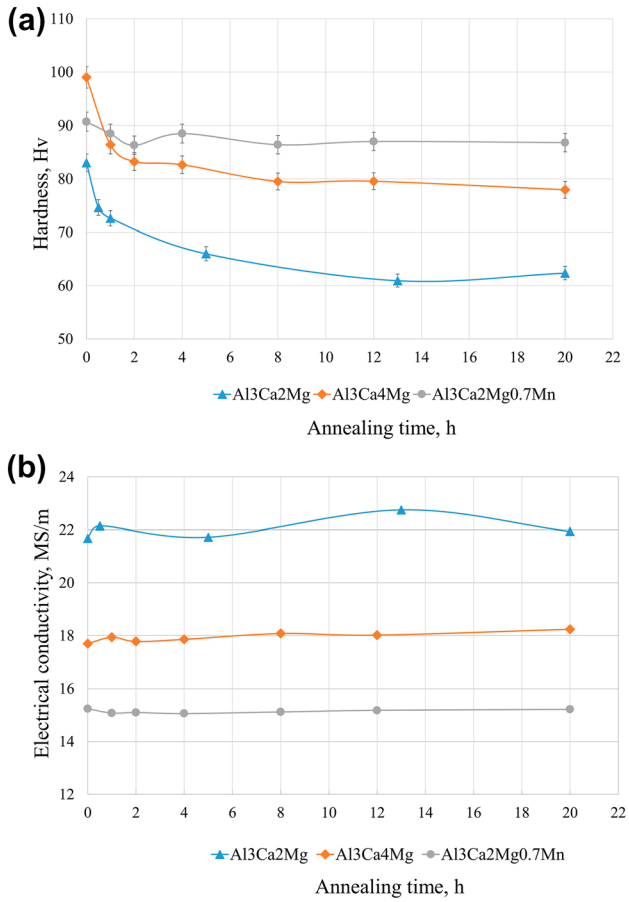

Fig. 6. Dependence of (a) hardness and (b) electrical conductivity on time during annealing at 250°C of the hot-rolled sheets (point "0" denotes as-wrought state).

is typical of the Al-Mg-based alloys[34] and comes from the interaction between solute Mg atoms and mobile dislocations.[34,35] Comparison of the strength of the Al3Ca2Mg and Al3Ca4Mg alloys revealed close yield strengths (YS) of 230 MPa and 250 MPa (Fig. 7c), respectively, and a slightly higher ultimate tensile strength (UTS) of the Al3Ca4Mg alloy, 340 MPa versus 300 MPa (Fig. 7b). The latter fact is associated with a more intense strain hardening in the highly alloyed alloy. Addition of 0.7% Mn affects the strength properties at room temperature only slightly. However, as shown above, the influence of Mn on the mechanical properties is noticeable at high temperatures. The base hot-rolled Al_4Mg alloy showed significantly lower strength properties compared to those of the new Ca-containing ones. Indeed, while the UTS is lower by about 25% (~ 240 MPa vs average 320 MPa), the difference in YS is much greater: ~ 90 MPa vs average 240 MPa. However, the relative elongation of the binary alloy is about seven times those of the Ca-containing ones (Fig. 7d). The high elongation of the base alloy originates from its low strength properties. However, the slight increase in the strength, which is observed for the ternary Al4Mg0.2Zr alloy after hot rolling, leads to an about twofold drop in the elongation. Thus, the observed drop in the elongation for the new Ca-containing alloys is associated with a natural decrease in the ductility with an increase in the strength. Further optimization of either processing modes or alloy composition can improve the combination of properties.

DISCUSSION

As shown above, addition of Ca in the Al-Mg alloys leads to a substantial increase in the strength properties of the hot-rolled sheets. To determine the reasons behind that result, the influence of different mechanisms on the YS was further considered in detail for the ternary Al3Ca2Mg alloy. Assuming that different strengthening mechanisms such as solid solution strengthening (σ_{ss}), grain boundary strengthening (σ_{gb}), dislocation strengthening (σ_ρ) and second phase strengthening (σ_p) have independent contributions to the YS of the alloy, the latter parameter can be calculated as follows:[36]

$$YS = \sigma_0 + \sigma_{ss} + \sigma_{gb} + \sigma_\rho + \sigma_p, \quad (1)$$

where σ_0 is the intrinsic resistance of the lattice to dislocation motion, which is approximately 20 MPa for most aluminum alloys.

The solid solution strengthening σ_{ss} caused by Mg can be calculated as follows:[35,36]

$$\sigma_{ss} = AC^\beta, \quad (2)$$

where C is the solute concentration in wt.%, and A and β are the constants equal to 13.3 MPa/(wt.%) and 1.19, respectively.[36–38] Considering that C = 2 wt.% for the alloy considered, σ_{ss} is ~ 30 MPa.

The contribution of grain boundary strengthening to YS can be calculated by the Hall-Patch equation, which can be expressed as follows:[39–42]

$$\sigma_{gb} = kD^{-1/2}, \quad (3)$$

where k = 0.17 MPa $m^{1/2}$ is the Hall-Petch coefficient[41] and D is the average grain or sub-grain sizes. From the data of structure analysis, the average size of sub-grain boundaries can be taken as about 1 μm (Fig. 5c and d). From the latter fact, σ_{gb} is ~ 190 MPa.

Dislocation strengthening can be determined as follows:

$$\sigma_\rho = M\alpha Gb\rho^{1/2}, \quad (4)$$

where M is Taylor's factor, α is a constant usually taken as 0.33,[38] G = 25.4 GPa is the shear modulus,[43] b = 0.286 nm is the Burgers vector, and ρ is

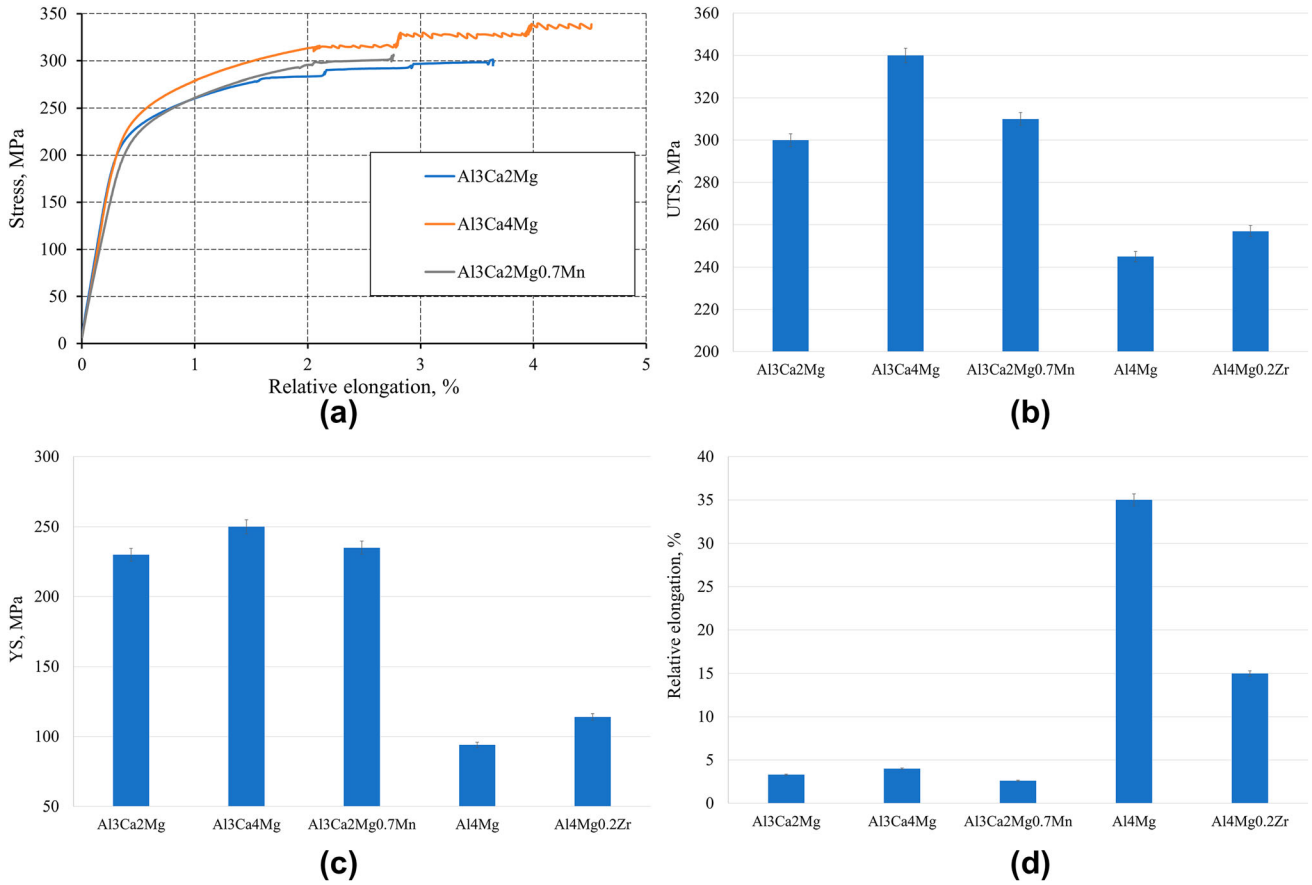

Fig. 7. (a) Characteristic tensile stress-strain diagrams of hot-rolled 2 mm sheets of experimental alloys and extracted data on (b) UTS, (c) YS and (d) relative elongation (%).

the dislocation density. The typical dislocation density for the hot-rolled aluminum alloys can be accepted at an order of 10^{11}–10^{12} m^{-2},[4] which has a rather insignificant effect on hardening varying in a range of 2.3–7.3 MPa, respectively.

Particle hardening σ_p caused by the Al_4Ca eutectic phase can be assessed using the Orowan equation,[44] and its contribution can be found as follows Eq. 5:

$$\sigma_p = \sqrt{3}\frac{Gb}{\lambda}, \quad (5)$$

However, given the relatively large average diameter of the intermetallic particles (can be taken 1.5 μm), this contribution can be neglected.

Figure 8 shows the obtained calculated data which allow one to assess the contributions of different strengthening mechanisms to the total YS. The calculated result of YS is presented in comparison with experimental data. The obtained data suggest that the calculated YS value of 227 MPa is very close to the experimental 230 MPa one. It is also can be seen that the contribution of sub-grain boundaries to strengthening is the main one and greatly exceeds the other contributions. The contribution of solid solution strengthening is the second one and is about 30 MPa, while for the Al4Mg alloy, according to Eq. 2, this value is about 70 MPa. For the Ca-free alloy, solid solution strengthening should be the main mechanism which in general corresponds well to the observed low value of the YS (Fig. 7b) of the

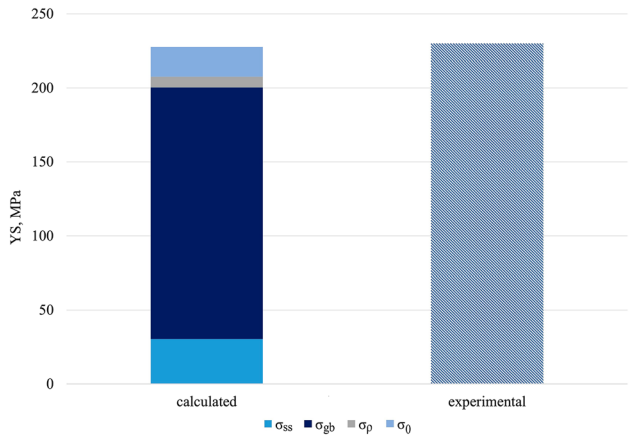

Fig. 8. Comparison of calculated and measured yield strength for hot-rolled Al3Ca2Mg alloy and contributions of different strengthening mechanisms to the total YS.

binary Al4Mg alloy. Thus, one can conclude from the analysis above that addition of eutectic forming calcium allows one to increase the strength properties of the wrought material through the stabilization of the sub-grain structure.

CONCLUSION

Analysis of the structure and mechanical properties of the new group of wrought alloys based on the Al-Ca-Mg system gave the following main results:

1. The experimental Al-3%Ca-(2-4)%Mg alloys were subjected to hot rolling at 400–450°C (depending on the actual magnesium content) without preliminary homogenization. The obtained high-quality sheet metal with a thickness of 2 mm (total degree of deformation 80%) confirms the high processability of the new materials.
2. Hot rolling leads to the formation of a composite structure consisting of relatively fine intermetallic particles of the eutectic Al_4Ca phase homogeneously distributed in the aluminum matrix saturated with magnesium. Deformation processing leads to the formation of a fine subgrains structure with a typical sub-grain size of 1 μm. Very fine crystals of the Al_4Ca phase particles are found at sub-grain boundaries, confirming their high pinning ability.
3. Tensile tests of the as-wrought alloys revealed the strength properties of the new alloys in a range of 230–250 MPa for the YS and 300–340 MPa for the UTS at a moderate ductility of $\sim$ 3–5%. Comparison with earlier data on the mechanical properties of the hot-rolled Al4Mg alloy having a strength that is typical for the Al-Mg group alloys (UTS 240 MPa, YS 90 MPa) revealed that Ca addition dramatically increases the strength of the Al-Mg alloys.
4. Detailed analysis of various mechanisms influencing the strengthening of the Al3Ca2Mg alloy revealed that the contribution of sub-grain boundaries is the largest and greatly exceeds all the others: its contribution to the total YS is $>$ 60%. Thus, addition of eutectic forming calcium in wrought Al-Mg alloys allows one to increase the strength properties through the stabilization of the sub-grain structure.

ACKNOWLEDGEMENTS

The study was carried out with the financial support of the grant of the Russian Science Foundation No. 22-19-00121 (https://rscf.ru/project/22-19-00121/) (alloy preparation, SEM, hot rolling, tensile tests and hardness analysis) and federal academic leadership program Priority 2030 of NUST MISIS (TEM, Discussion).

DATA AVAILABILITY

The raw/processed data required to reproduce these findings cannot be shared at this time because of technical or time limitations.

CONFLICT OF INTEREST

On behalf of all authors, the corresponding author states that there is no conflict of interest.

REFERENCES

1. J. Hirsch, *Mater. Trans.* https://doi.org/10.2320/matertrans.L-MZ201132 (2011).
2. K. Zheng, D.J. Politis, L. Wang, and J. Lin, *Int. J. Lightweight Mater. Manuf.* https://doi.org/10.1016/j.ijlmm.2018.03.006 (2018).
3. J. Hirsch, *Trans. Nonferrous Met. Soc. China*. https://doi.org/10.1016/S1003-6326(14)63305-7 (2014).
4. I.J. Polmear, *Light Alloys: From Traditional Alloys to Nanocrystals* (Butterworth-Heinemann, Oxford, 2006), p421.
5. R.G. Guan and D. Tie, *Acta Metall. Sin.* https://doi.org/10.1007/s40195-017-0565-8 (2017).
6. D.H. Jang, Y.B. Park, and W.J. Kim, *Mater. Sci. Eng. A*. https://doi.org/10.1016/j.msea.2018.11.132 (2019).
7. J.E. Hatch, *Aluminium: Properties and Physical metallurgy* (American Society for Metals, Ohio, 1984), p424.
8. R. Guan, D. Tie, Z. Li, Y. An, X. Wang, Q. Li, and X. Chen, *Mater. Sci. Eng. A*. https://doi.org/10.1016/j.msea.2018.09.090 (2018).
9. N.A. Belov, E.A. Naumova, A.N. Alabin, and I.A. Matveeva, *J. Alloys Compd.* https://doi.org/10.1016/j.jallcom.2015.05.155 (2015).
10. E. Naumova, V. Doroshenko, M. Barykin, T. Sviridova, A. Lyasnikova, and P. Shurkin, *Metals*. https://doi.org/10.3390/met11060890 (2021).
11. T.K. Akopyan, N.A. Belov, A.A. Lukyanchuk, N.V. Letyagin, T.A. Sviridova, A.N. Petrova, A.S. Fortuna, and A.F. Musin, *Mater. Sci. Eng. A*. https://doi.org/10.1016/j.msea.2020.140633 (2021).
12. S.O. Rogachev, E.A. Naumova, A.V. Doroshenko, R.D. Karelin, V.S. Komarov, V.S. Yusupov, NYu. Tabachkova, V.A. Andreev, and V.M. Khatkevich, *J. Alloys Compd.* https://doi.org/10.1016/j.jallcom.2022.165379 (2022).
13. N.A. Belov, D.G. Eskin, and A.A. Aksenov, *Multicomponent Phase Diagrams: Applications for Commercial Aluminium Alloys* (Elsevier, Amsterdam, 2005), p424.
14. N.A. Belov, E.A. Naumova, T.K. Akopyan, and V.V. Doroshenko, *JOM*. https://doi.org/10.1007/s11837-018-2948-3 (2018).
15. N. Belov, T. Akopya, N. Korotkova, M. Murashkin, V. Timofeev, and A. Fortuna, *Metals*. https://doi.org/10.3390/met11020236 (2021).
16. N.A. Belov, T.K. Akopyan, N.O. Korotkova, E.A. Naumova, A.M. Pesin, and N.V. Letyagin, *JOM*. https://doi.org/10.1007/s11837-020-04342-x (2020).
17. T.K. Akopyan, N.V. Letyagin, N.A. Belov, A.N. Koshmin, and D.S.H. Gizatulin, *Phys. Met. Metallogr.* https://doi.org/10.1134/S0031918X20080025 (2020).
18. N.A. Belov, E.A. Naumova, T.K. Akopyan, and V.V. Doroshenko, *Metals*. https://doi.org/10.3390/met7100429 (2017).
19. S. Zhang, H. Du, Z. Yao, Z. Liu, Y. Zhu, L. Shuai, T. Huang, X. Huang, X. Tao, D.P. Mondal, T. Akopyan, and N. Belov, *Mater. Sci. Eng. A*. https://doi.org/10.1016/j.msea.2022.143533 (2022).
20. V.V. Doroshenko, M.A. Barykin, N.O. Korotkova, and M.A. Vasina, *Phys. Met. Metallogr.* https://doi.org/10.1134/S0031918X22080038 (2022).

21. N.A. Belov, E.A. Naumova, T.A. Bazlova, and E.V. Alekseeva, *Phys. Met. Metallogr.* https://doi.org/10.1134/S0031918X16020046 (2016).
22. J.D. Boyd and R.B. Nicholson, *Acta Metall.* https://doi.org/10.1016/0001-6160(71)90076-9 (1971).
23. Information on www.thermocalc.com (2023). Accessed 30 May 2023.
24. J.O. Andersson, T. Helander, L. Höglund, P. Shi, and B. Sundman, *Calphad*. https://doi.org/10.1016/S0364-5916(02)00037-8 (2002).
25. T.K. Akopyan, N.V. Letyagin, T.A. Sviridova, N.O. Korotkova, and A.S. Prosviryakov, *JOM*. https://doi.org/10.1007/s11837-020-04340-z (2020).
26. T.K. Akopyan, N.A. Belov, E.A. Naumova, N.V. Letyagin, and T.A. Sviridova, *Trans. Nonferrous Met. Soc. China*. https://doi.org/10.1016/S1003-6326(20)65259-1 (2020).
27. M. Mofarrehi, M. Javidani, and X.G. Chen, *Mater. Sci. Eng. A*. https://doi.org/10.1016/j.msea.2022.143217 (2022).
28. X. Qian, N. Parson, and X.G. Chen, *J. Mater. Sci. Technol.* https://doi.org/10.1016/j.jmst.2020.04.015 (2020).
29. O. Engler, K. Kuhnke, and J. Hasenclever, *J. Alloys Compd.* https://doi.org/10.1016/j.jallcom.2017.09.060 (2017).
30. X. Qian, N. Parson, and X.G. Chen, *Mater. Sci. Eng.* https://doi.org/10.1016/j.msea.2019.138253 (2019).
31. Y.J. Li and L. Arnberg, *Acta Mater.* https://doi.org/10.1016/j.actamat.2004.02.015 (2004).
32. N.A. Belov, N.O. Korotkova, T.K. Akopyan, and K.A. Tsydenov, *Metals*. https://doi.org/10.3390/met9121246 (2019).
33. D. Joy, R. Aravindakshan, and N.S. Varrma, *Mater. Today Proc.* https://doi.org/10.1016/j.matpr.2021.05.284 (2021).
34. F. Bakare, L. Schieren, B. Rouxel, L. Jiang, T. Langan, A. Kupke, M. Weiss, and T. Dorin, *Mater. Sci. Eng. A*. https://doi.org/10.1016/j.msea.2021.141040 (2021).
35. Y. Cai, S. Yang, S. Fu, D. Zhang, and Q. Zhang, *J. Mater. Sci. Technol.* https://doi.org/10.1016/j.jmst.2016.05.012 (2017).
36. I. Vysotskiy, D. Zhemchuzhnikova, S. Malopheyev, S. Mironov, and R. Kaibyshev, *Mater. Sci. Eng. A*. https://doi.org/10.1016/j.msea.2019.138540 (2020).
37. H. Wang, H. Geng, D. Zhou, K. Niitsu, O. Mur´ansky, and D. Zhang, *Mater. Sci. Eng. A*. https://doi.org/10.1016/j.msea.2019.138613 (2020).
38. N. Kumar and R.S. Mishra, *Mater. Sci. Eng. A*. https://doi.org/10.1016/j.msea.2013.05.006 (2013).
39. A. Dubyna, A. Mogucheva, and R. Kaibyshev, *Adv. Mater. Res.* https://doi.org/10.4028/www.scientific.net/AMR.922.120 (2014).
40. D.J. Lloyd and S.A. Court, *Mater. Sci. Technol.* https://doi.org/10.1179/026708303225006088 (2013).
41. L. Jiang, Z. Zhang, Y. Bai, S. Li, and W. Mao, *Crystals*. https://doi.org/10.3390/cryst12050673 (2022).
42. D.J. Abson and J.J. Jonas, *Metal Sci. J.* https://doi.org/10.1179/msc.1970.4.1.24 (2013).
43. H. Du, S. Zhang, and B. Zhang, *J. Mater. Sci.* https://doi.org/10.1007/s10853-021-06310-5 (2021).
44. M. Zha, Y. Li, R.H. Mathiesen, R. Bjørge, and H.J. Roven, *Mater. Sci. Eng. A*. https://doi.org/10.1016/j.msea.2013.12.103 (2014).